The vibration-rotation-tunnelling spectrum of the polar and T-shaped-N-in isomers of $(NNO)_2$

Xiao-Gang Wang* and Tucker Carrington Jr.†

Chemistry Department, Queen's University,

Kingston, Ontario K7L 3N6, Canada

Richard Dawes‡

Missouri University of Science and Technology, Rolla, Missouri 65401, USA

Ahren W. Jasper§

Combustion Research Facility, Sandia National Laboratories,

P.O. Box 969, Livermore, California 94551, USA

(Dated: 18 Februrary 2011)

Abstract

In this paper we report transition frequencies and line strengths computed for bright states of the NNO dimer. We use a previously reported potential obtained from explicitly correlated coupled-cluster calculations and fit using an interpolating moving least squares method. The rovibrational Schroedinger equation is solved with a symmetry adapted Lanczos algorithm and an uncoupled product basis set. All four intermolecular coordinates are included in the calculation. We propose two tools for associating rovibrational wavefunctions with vibrational states and use them to find polar-like and T-shaped-N-in-like rovibrational states. The first tool uses a re-expansion of the rovibrational wavefunction in terms of $J = 0$ eigenfunctions. The second uses intensities. Calculated rotational transition frequencies are in very close agreement with experiment.

*Electronic address: xgwang.dalian@gmail.com

†Electronic address: Tucker.Carrington@queensu.ca,Fax:613-533-6669

‡Electronic address: dawesr@mst.edu

§Electronic address: ajasper@sandia.gov

I. INTRODUCTION

The spectroscopy of $(NNO)_2$ has interested experimentalists and theorists for many years. [1–14] $(NNO)_2$ is a loosely bound Van der Waals complex of the type that has interested McKellar and his co-workers. [1–3, 15–18] It has important large amplitude motions of the type that have interested Bunker and his co-workers. [19–27] The deepest minimum on the $(NNO)_2$ potential energy surface (PES) corresponds to a non-polar slipped-antiparallel structure with C_{2h} symmetry. Spectra attributed to the ν_2 and ν_3 fundamentals and to the $\nu_2 + \nu_3$ combination band (intra-molecular modes) were observed. [6, 7] Also observed were combination bands involving the (inter-molecular) torsion and disrotatory coordinates. [2, 5, 9] Transitions among states associated with a polar isomer (or isomers) of $(NNO)_2$ have also recently been observed. [1, 3] As discussed in Ref. 13 (hereafter denoted paper I) and Ref. 14 there are two polar isomers and both have a slipped-parallel structure with C_s symmetry. A microwave spectrum of the polar isomer was also recorded. [4] In this paper we use an accurate PES and compute rovibrational spectra considering the four inter-molecular coordinates. In paper I we presented the PES and energy levels associated with the global non-polar minimum. In this paper we present intensities and focus on understanding the microwave spectrum of the polar isomer. There have been several theoretical studies of $(NNO)_2$ using various levels of ab initio theory to determine structures and harmonic frequencies of the possible isomers. In particular, Berner et al. used the (CCSD/aug-cc-pVDZ) method. [9] They stress the importance of the disrotatory cycle.

The potential surface has local wells for both the polar and the T-shaped N-in (TN) shapes. There are two equivalent wells for both the polar and the TN shapes. The questions that are the focus of this paper are: (1) Are there vibrational states that are localized in the local minima (polar and TN) ? How does one identify polar-like and TN-like rovibrational states if they exist? (2) To what extent are the intensities of transitions between polar-like rovibrational states determined by the selection rules one would expect if the complex were rigid and had the shape corresponding to the bottom of a polar well? (3) Does tunnelling between equivalent wells give rise to splittings that might be observable? Some of these questions were addressed in a recent paper. [14] The potential used in Ref. 14 has no or perhaps very shallow TN minima and no TN states were reported, but some of polar-like

states of Ref. 14 are close to those we obtain. Ref. 14 does not present intensities or discuss how to identify $J > 0$ polar-like states.

We find polar-like states and propose two tools for identifying their associated vibrational states. Polar-like states are expected owing to the fact that microwave transitions were observed[4] and assigned to the polar isomer. The first tool uses intensities. Transitions between polar-like and TN-like rovibrational states are bright, but transitions between other rovibrational states are not. States linked by weak transitions, i.e. dark states, all have have significant amplitude in the global minimum well. The second tool uses a re-expansion of the $J > 0$ wavefunctions in the basis of $J = 0$ eigenfunctions.

II. POTENTIAL ENERGY SURFACE

A four-dimensional (rigid monomer) potential energy surface was made using an interpolating moving least-squares fitting method. 1757 *ab initio* points computed at the CCSD(T)-F12b/VTZ-F12 level [28] were used to produced a surface with an estimated fitting error of less than 1.5 cm^{-1}. Details were discussed in paper I. In this section, we summarize the features related to the tunnelling dynamics between the two equivalent polar wells.

The coordinates used to compute the rovibrational levels and wavefunctions were described in paper I. They are r_0, the distance between the two monomers, the standard polyspherical angles $(\theta_1, \theta_2, \phi_2)$, and the Euler angles (α, β, γ). [29–32] The nature of the large-amplitude motion is more easily understand using the extended angles $(\tilde{\theta}_1, \tilde{\theta}_2)$ defined by extending the range of (θ_1, θ_2) from $[0, \pi]$ to $[0, 2\pi]$. They were used by Hougen and Ohashi for HF dimer[33]. The disrotatory (X) and conrotatory (Y) coordinates are easily defined in terms of the extended angles: $X = (\tilde{\theta}_1 + \tilde{\theta}_2)/2$ and $Y = (\tilde{\theta}_1 - \tilde{\theta}_2)/2$. Fig. 1 is a contour diagram of the potential. For each pair of values (θ_1, θ_2) the potential is minimized with respect to r_0 for both $\phi_2 = 180°$ and $\phi_2 = 0°$. The two polar wells are in the lower panel of Fig. 1. Starting from the polar well at $(\theta_1 \approx 120°, \theta_2 \approx 120°)$ one moves counterclockwise around the disrotatory cycle, from one polar structure to the other, by following the potential valley to the T shaped structure at $(\theta_1 \approx 180°, \theta_2 \approx 90°)$ and then moving to the upper panel, proceeding to the N-in non-polar structure, denoted NN on the plot, and moving back to the lower panel and along to the polar minimum at $(\theta_1 \approx 60°, \theta_2 \approx 60°)$. The

same path is shown in the extended coordinates in Fig. 2. In this case it is only necessary to exit and enter once to follow the path between the two polar minima P1 and P2 (P3 and P4 are copies). The full disrotatory cycle (Fig. 3), as first shown by Berner *et al.*[9], goes from the global minimum (non-polar O-in) (G1), to a T-shaped O-in (TO1) transition state, to a polar well (P1), to a T-shaped N-in (TN1) well, to the non-polar N-in transition state (NN1), to a TN2 well, to the P2 well, through a TO2 transition state, and finally back to G1.

Three tunnelling paths connect the two polar wells. Two of them follow the disrotatory cycle, one in a clockwise sense and one in an anticlockwise sense. The first path (called disrotatory path I) is P1 $\rightarrow$ TO1 $\rightarrow$ G1 $\rightarrow$ TO2 $\rightarrow$ P2. The second path (called disrotatory path II) is P1 $\rightarrow$ TN1 $\rightarrow$ NN1 $\rightarrow$ TN2 $\rightarrow$ P2. These two paths are marked by dashed arrows in Fig. 3. The third path is conrotatory (Fig. 4). It is P1 $\rightarrow$ RT $\rightarrow$ P3. When the path is defined by finding values of X and r_0 that minimize the potential for each value of Y the RT transition state is approximately rectangle-shaped. Its coordinates are $\theta_1 = 91.9^\circ$, $\theta_2 = 88.1^\circ$, and $r_0 = 6.996$ bohr. The blue contours of Fig. 1 reveal RT. The RT shape is not an exact rectangle and therefore its point group symmetry is not C_{2v} but rather C_s, the same as other points along this path. The energetics of the various stationary points are given in Table I. Geometries of all the stationary points except RT are also given in Table V of paper I. The barrier height for disrotatory path I is 105 cm^{-1} (TO). The barrier height for disrotatory path II is 142 cm^{-1} (NN). The barrier height for the conrotatory path is 400 cm^{-1} (RT). The width of the conrotatory barrier is much less than the width of the barrier of disrotatory path II. Disrotatory path I has two barriers.

It is not clear that only one of the three paths is important and therefore the tunnelling dynamics could be quite complicated. This may be contrasted with the tunnelling in HF dimer where one disrotatory path is the dominant path. Mills[34] and also Hougen and Ohashi concluded[33] that if one tunnelling path is dominant the symmetry of a vibration-rotation-tunnelling level is a product of the symmetry of a rotational factor, determined assuming a rigid shape with the symmetry of the point group of the transition state shape, and the symmetry of a vibrational/tunnelling factor. According to our calculation the tunnelling splittings are very small, primarily because the mass of the monomer is relatively large. Even if it were possible to identify one or more paths as being more important, doing

so would have no consequences for understanding the spectrum.

III. CALCULATING ENERGY LEVELS AND WAVEFUNCTIONS

The polyspherical coordinates defined in the previous section are used to compute the energy levels. Details were given in Paper I. Euler angles specify the orientation of a body-fixed frame attached such that the z-axis is along $\mathbf{r_0}$ and the x-axis is along the vector $\mathbf{r_0} \times \mathbf{r_1} \times \mathbf{r_0}$. $\mathbf{r_0}$ is the inter-monomer vector and $\mathbf{r_1}$ is the vector along monomer 1, pointing from the external N atom to O atom. The kinetic energy operator in these coordinates is well known. [35] For the stretch coordinates we use potential optimized discrete variable representation (PODVR) functions [36–41] and for the bend and rotational coordinates we use parity adapted rovibrational functions [30, 31] In our calculations the angular quantum numbers (see paper I) l_1, l_2, and m_2 all have the same maximum value. Even and odd parity levels are calculated separately.

Within each parity block, we use a symmetry adapted variant [42–44] of the Cullum and Willoughby Lanczos method [45] to compute the energy levels. Eigenvalues are obtained by computing matrix-vector products. Potential matrix-vector products are evaluated by using quadrature and doing sums sequentially. [37, 44, 46–48] Kinetic energy matrix-elements are given in Ref. 35. The wavefunctions are obtained from eigenvectors of the Hamiltonian matrix that are computed as described previously. [30, 49] Similar techniques have been used to compute energy levels of many molecules. [37, 50–53] The full permutation-inversion (PI) symmetry group for the Hamiltonian we use is G_4, composed of operations $\{E, \sigma_{ex}\} \otimes \{E, E^*\}$ where σ_{ex} permutes monomer 1 with monomer 2. [19] A/B label symmetric and antisymmetric irreducible representations (irreps) with respect to σ_{ex} and $+/-$ label even and odd parities. There are four PI irreps: $(A+, B+, A-, B-)$. Transformation properties of parity-adapted rovibrational basis functions under G_4 operators are given in Ref. 54. The dipole moment of the complex has $A-$ symmetry. Allowed transitions are therefore $A+ \leftrightarrow A-$ and $B+ \leftrightarrow B-$. For the results presented in the section VI we use the basis, quadrature points, masses and NNO rotational constant used in paper I.

IV. IDENTIFYING ROVIBRATIONAL STATES ASSOCIATED WITH POLAR-LIKE OR TN-LIKE VIBRATIONAL STATES

When coupling between vibration and rotation is not too strong, each rovibrational wavefunction can be approximated as a product of a vibrational wavefunction and a rotational function. The vibrational wavefunction associated with a rovibrational state can be determined on the basis of the energy level pattern, if all vibrational levels are widely-spaced. Energy levels are calculated separately for each J and for each J one can identify groups of 1, 3, 5, $\cdots$ rotational levels. This simple procedure fails when rotational and vibrational energy levels are similar, i.e., when the density of vibrational states is large. Note that although the density of vibrational states may make it impossible to determine the vibrational wavefunction associated with a rovibrational state, it does not necessarily invalidate the product approximation. The simple procedure also fails whenever there are groups of nearly degenerate levels such as when there are small tunnelling splittings. There are two situations in which, even in the presence of tunnelling, one can easily identify the vibrational/tunnelling state associated with a rovibrational level. (i) there is only one tunnelling path and one knows the symmetry at the transition state (e.g NH_3) (ii) the tunnelling splitting is not tiny and there are several possible tunnelling paths but only one is important (e.g. HF dimer). In situation (ii), if one knows transition frequencies for transitions from both tunnelling partners then symmetry selection rules alone enable one to determine whether to associate the upper or the lower tunnelling state with a specific rovibrational state. If not all the transitions are available then it is necessary to also use estimated rotational constants. [55] In NNO dimer we have the density of states problem when attempting to attribute rovibrational states to polar-like vibrational states and NNO dimer also has several possible tunnelling paths and tiny tunnelling splittings. We therefore need alternatives to the simple energy level pattern procedure. They will enable us to determine whether a rovibrational transition is between different tunnelling states or within the same tunnelling state. In the latter case, it is a pure rotational transition and this transition is described as *within*. In the former case the transition is described as *across*.

A. The vibrational parent of a $J > 0$ level

We denote the vibrational state associated with a specific rovibrational state its vibrational parent. The first tool we have developed for finding the parent uses a re-expansion of the rovibrational wavefunction. The idea is closely related to a procedure used in Ref. 56. Results for NNO dimer are presented in the next section; the idea has also been tested and shown to work on HF dimer and H_2O_2.

Given a rovibrational wavefunction,

$$\Psi^{(J)} = \sum_{l_1,l_2,m_2;K} c_{l_1,l_2,m_2;K} |l_1, l_2, m_2(K)\rangle |JK\rangle \tag{1}$$

and a set of vibrational wavefunctions,

$$\Phi_v = \sum_{l_1,l_2,m_2} d_{l_1,l_2,m_2} |l_1, l_2, m_2\rangle \ , \tag{2}$$

one can re-expand the rovibrational wavefunction in the vibrational wavefunction basis, by inserting $\sum_v |\Phi_v\rangle\langle\Phi_v| = 1$ into Eq. (1) to obtain,

$$\Psi^{(J)} = \sum_{v,K} \tilde{c}_{K,v} |\Phi_v\rangle |JK\rangle \ , \tag{3}$$

where

$$\tilde{c}_{K,v} = \sum_{l_1,l_2,m_2} c_{l_1,l_2,m_2;K} \langle \Phi_v | l_1, l_2, m_2(K)\rangle \ . \tag{4}$$

The contribution of state Φ_v to state $\Psi^{(J)}$ is given by

$$P_v = \sum_K \tilde{c}^2_{K,v} \ . \tag{5}$$

The vibrational state with the largest P_v is considered to be the vibrational parent of the rovibrational state $\Psi^{(J)}$. Note that the body-fixed frame of the Wigner function $|JK\rangle$ in Eq. (3) is the same as the body-fixed frame of the original basis (Eq. (1)). That frame may not be the best for the purpose of separating vibration and rotation in Eq. (3), however, this should be unimportant because of the sum over K in the equation for P_v.

The overlap integral in Eq. (4) is a vibrational integral. (K) indicates that the vibrational basis depends on K (because $m_1 = K - m_2$). When Φ_v is replaced with the right side of Eq. (2) one obtains an overlap integral of associated Legendre polynomials,

$$\langle l_1', l_2', m_2'(K'=0) | l_1, l_2, m_2(K)\rangle = \delta_{l_2',l_2} \delta_{m_2',m_2} \langle \Theta^{(-m_2)}_{l_1'} | \Theta^{(K-m_2)}_{l_1} \rangle \ . \tag{6}$$

$\langle \Theta_{l_1'}^{(-m_2)} | \Theta_{l_1}^{(K-m_2)} \rangle$ is an integral over θ_1 and is computed numerically exactly with Gauss quadrature. Note that if the vibrational basis label (m_1) is independent of K, then the integral in Eq. (6) is a Kronecker delta and it becomes simpler to calculate P_v. For example, Mátus *et al.* [56] use a vibrational (normal mode) basis that does not depend on rotational quantum numbers.

B. Identifying states via intensities

Computed intensities can also be used to identify polar-like vibrational states and rovibrational states associated with polar-like vibrational states. To compute intensities one needs a dipole surface. We use a simple model. The equations necessary for calculating intensities are given in the next section. In this subsection we explain how intensities are used to identify states. A transition between two rovibrational states will be intense if both of the rovibrational states are associated with vibrational states with significant amplitude in the polar or TN wells. We refer to such states as bright states. We therefore compute $R(0)$ line strengths for transitions between all $J = 0$ levels and all $J = 1$ levels and identify the states connected by strong transitions as being associated with polar-like or TN-like vibrational states. The idea is illustrated in Fig. 5. Most line strengths are nearly zero, implying that most states are localized in the non-polar well. The lowest-energy bright states we find are associated with states whose vibrational parent, determined using the procedure of the previous subsection, is a polar-like state. By plotting $J = 0$ wavefunctions we confirm that all the $J = 0$ states with bright $R(0)$ transitions have significant amplitude outside the non-polar well.

V. INTENSITY CALCULATION

At the global potential minimum, $(NNO)_2$ has a slipped anti-parallel structure with C_{2h} point group symmetry and no dipole moment. If $(NNO)_2$ were rigid and had the global minimum shape it would have no microwave (MW) transitions. According to the potential of paper I([13]) there are two important types of local minima: the polar minima with a slipped approximately parallel structure and T-shaped N-in (TN) minima where the two

monomers are approximately perpendicular to each other with the N atom of one of the monomers pointing towards the other monomer. All of these local minima have structures with permanent dipoles. If $(NNO)_2$ were rigid and had one of these local minimum shapes it would have MW transitions. $(NNO)_2$ is of course not rigid; at least some of its wavefunctions have nonzero amplitude in the local minima wells. Accurate intensities can be determined by computing wavefunctions and dipole moment integrals.

To compute intensities it is convenient to use the equations presented in Ref. 57. In that paper the equations are written using angles that relate a monomer fixed (MF) axis system to a dimer-fixed (DF) axis system attached to the inter-monomer vector, which in turn is related to the space-fixed (SF) axis system by two Euler angles . In this paper the basis functions used (see section III and paper I) to compute the energy levels and wavefunctions are in terms of polyspherical coordinates. To use the equations of Ref. 57 one therefore needs to link the two sets of angles. The non-parity-adapted angular basis function used in paper I is a product of a spherical harmonic and a Wigner function[58],

$$|\Phi_1\rangle = |l_1(m_1)l_2m_2; JKM\rangle = \sqrt{\frac{2J+1}{8\pi^2}}\Theta_{l_1}^{m_1}(\theta_1)Y_{l_2}^{m_2}(\theta_2,\phi_2)D_{MK}^{J}(\alpha,\beta,\gamma)^* \tag{7}$$

with

$$\begin{aligned} Y_{l_2}^{m_2}(\theta_2,\phi_2) &= \frac{1}{\sqrt{2\pi}}\Theta_{l_2}^{m_2}(\theta_2)e^{im_2\phi_2} \\ m_1 &\equiv K - m_2 \ , \end{aligned} \tag{8}$$

where $\Theta_l^m(\theta)$ is a normalized associated Legendre function with the $(-1)^m$ Condon-Shortley phase factor. D_{MK}^J is a Wigner function [58] and (α,β,γ) are the Euler angles that define a three-angle body-fixed (BF) frame whose z-axis is along the vector $\mathbf{r_0}$ and whose x-axis is along vector $\mathbf{r_0}\times\mathbf{r_1}\times\mathbf{r_0}$. Alternatively one can study $(NNO)_2$ using the two-angle DF frame and uncoupled basis functions similar to those used for $(H_2O)_2$. [59–62] Monomer fixed (MF) frames attached to the monomers are specified by two Euler angles $(\alpha_\sigma,\beta_\sigma)$, for each monomer, $\sigma = A, B$, that relate the DF and MF frames. [59] The $z-$axes of the MF frames are aligned with the linear monomers parallel to $\mathbf{r_1}$ and $\mathbf{r_2}$. Appropriate basis functions are obtained from the uncoupled basis of $(H_2O)_2$ by setting $\gamma_A = \gamma_B = 0$, and $k_A = k_B = 0$. The uncoupled basis functions are,

$$|\Phi_2\rangle = |j_A(m_A); j_Bm_B; JKM\rangle$$

$$= \sqrt{\frac{2j_A+1}{4\pi}}\sqrt{\frac{2j_B+1}{4\pi}}\sqrt{\frac{2J+1}{4\pi}} D^{j_A}_{m_A0}(\alpha_A,\beta_A,0)^* D^{j_B}_{m_B0}(\alpha_B,\beta_B,0)^* D^{J}_{MK}(\alpha,\beta,0)^*$$

$$= \left(\frac{1}{\sqrt{2\pi}}\right)^3 \bar{d}^{j_A}_{m_A0}(\beta_A)\bar{d}^{j_B}_{m_B0}(\beta_B)\bar{d}^{J}_{MK}(\beta) e^{i(M\alpha+m_A\alpha_A+m_B\alpha_B)} \tag{9}$$

with $\bar{d}^j_{mk}(\beta) = \sqrt{(2j+1)/2} d^j_{mk}(\beta)$ being a normalized Wigner d-function and the constraint

$$m_A \equiv K - m_B \ . \tag{10}$$

This constraint makes the kinetic energy operator (KEO) singularity-free. Now using the relation

$$m_A\alpha_A + m_B\alpha_B = (m_A+m_B)\alpha_A + m_B(\alpha_B-\alpha_A) \tag{11}$$

and $\bar{d}^j_{m0}(\beta) = \Theta^m_j(\beta)$, one finds,

$$|\Phi_2\rangle = \sqrt{\frac{2J+1}{8\pi^2}} \Theta^{m_A}_{j_A}(\beta_A) Y^{m_B}_{j_B}(\beta_B, \alpha_B-\alpha_A) D^J_{MK}(\alpha,\beta,\alpha_A)^* \ . \tag{12}$$

Recognizing that the polyspherical angles are related to the angles based on the DF frame by

$$\theta_1 = \beta_A;\ \theta_2 = \beta_B;\ \phi_2 = \alpha_B - \alpha_A;\ \gamma = \alpha_A \ , \tag{13}$$

replacing

$$l_1 = j_A \ ; m_1 = m_A \ ; l_2 = j_B \ ; m_2 = m_B \ , \tag{14}$$

we find that

$$|\Phi_1\rangle = |\Phi_2\rangle \ . \tag{15}$$

The wavefunctions we compute with the coordinates and basis functions of paper I can therefore be used with the intensity equations of Ref. 57

The line strength is

$$S_{i'i} = 3\left|\sum_{M,M'} \langle\Psi_{i'}|\mu_0^{\rm SF}|\Psi_i\rangle\right|^2 \ , \tag{16}$$

where $\mu_0^{\rm SF} = \mu_Z^{\rm SF}$ is the space-fixed Z component of the dipole moment operator and Ψ_i is a rovibrational wavefunction. [19] The simple and realistic dipole model we use for $(NNO)_2$ replaces $\mu_0^{\rm SF}$ with a sum of two terms, one for each monomer. Each term is a dipole parallel to one of the two linear monomers and each term can be written in terms of DF frame dipole components

$$\mu_0^{\rm SF} = \sum_{\sigma=-1}^{1} D^{(1)}_{0,\sigma}(\alpha,\beta,0)^* \mu_\sigma^{\rm DF} \tag{17}$$

For the term associated with monomer A and in terms of the angles defining the MF frame of monomer A, $(\alpha_A, \beta_A, 0)$, we have

$$\mu_\sigma^{\rm DF} = \sum_{\sigma'=-1}^{1} D^{(1)}_{\sigma,\sigma'}(\alpha_A, \beta_A, 0)^* \mu_{\sigma'}^{\rm MF} \ , \tag{18}$$

and

$$\mu_0^{\rm SF} = \sum_{\sigma,\sigma'=-1}^{1} D^{(1)}_{0,\sigma}(\alpha, \beta, 0)^* D^{(1)}_{\sigma,\sigma'}(\alpha_A, \beta_A, 0)^* \mu_{\sigma'}^{\rm MF} \ . \tag{19}$$

Because the dipole moment of NNO is along the MF z-axis, $\mu_1^{\rm MF} = \mu_{-1}^{\rm MF} = 0$ and $\mu_0^{\rm MF} = \mu_{\rm NNO}$. Therefore Eq. (19) is simplified,

$$\mu_0^{\rm SF} = \mu_{\rm NNO} \sum_{\sigma=-1}^{1} D^{(1)}_{0,\sigma}(\alpha, \beta, 0)^* D^{(1)}_{\sigma,0}(\alpha_A, \beta_A, 0)^* \ . \tag{20}$$

To compute line strengths we must compute $\langle \Psi_{i'} | \mu_0^{\rm SF} | \Psi_i \rangle$, where $\mu_0^{\rm SF}$ is replaced with a sum of the right hand side of Eq. (20) and a similar equation for the contribution of monomer B. Refs. 63–65 give equations for computing these integrals in a coupled rovibrational basis. We prefer the uncoupled basis (Eq. (9)) because it simplifies computing matrix-vector products. It is equivalent to the basis of Eq. (7), used to compute the energy levels and wavefunctions. The wavefunctions Ψ_i computed in the parity-adapted basis need to be written in terms of the non-parity-adapted basis. To compute line strengths one then requires matrix elements of the operator of Eq. (20) in the non-parity-adapted basis of Eq. (9)[19, 58]. For one of the monomer contributions the required integral is,

$$\begin{aligned} & \langle j'_A(m'_A); j'_B m'_B; J'K'M' | \mu_0^{\rm SF} | j_A(m_A); j_B m_B; JKM \rangle \\ = \ & \mu_{\rm NNO} \delta_{j'_B, j_B} \delta_{m'_B, m_B} \sum_{\sigma=-1}^{1} (-1)^{m'_A} [j'_A][j_A] \begin{pmatrix} j'_A & 1 & j_A \\ 0 & 0 & 0 \end{pmatrix} \begin{pmatrix} j'_A & 1 & j_A \\ -m'_A & \sigma & m_A \end{pmatrix} \\ \times \ & (-1)^{K'+M'} [J'][J] \begin{pmatrix} J' & 1 & J \\ -K' & \sigma & K \end{pmatrix} \begin{pmatrix} J' & 1 & J \\ -M' & 0 & M \end{pmatrix} \end{aligned} \tag{21}$$

where $[J] = \sqrt{2J+1}$ etc.

Rather than using dimer-type basis functions in terms of angles relating monomer frames and a two-angle embedded frame as is explained in the previous two paragraphs it is possible to directly derive the line strength expression using only the coordinates and basis functions of paper I. The result is equivalent, but not as compact. To proceed in this fashion $\mu_0^{\rm SF}$ is written as a linear combination of components in the three-angle BF frame,

$$\mu_0^{\rm SF} = \sum_{\sigma=-1}^{1} D^{(1)}_{0,\sigma}(\alpha, \beta, \gamma)^* \mu_\sigma^{\rm BF} \ . \tag{22}$$

The integral of $\mu_0^{\rm SF}$ in the basis of Eq. (7) is

$$\begin{aligned}
& \langle l_1'(m_1')l_2'm_2'; J'K'M'|\mu_0^{\rm SF}|l_1(m_1)l_2m_2; JKM\rangle \\
= & \sum_{\sigma=-1}^{1} \langle l_1'(m_1')l_2'm_2'|\mu_\sigma^{\rm BF}|l_1(m_1)l_2m_2\rangle \\
\times & (-1)^{K'+M'}[J'][J] \begin{pmatrix} J' & 1 & J \\ -K' & \sigma & K \end{pmatrix} \begin{pmatrix} J' & 1 & J \\ -M' & 0 & M \end{pmatrix} . \qquad (23)
\end{aligned}$$

A similar equation was derived by Le Sueur *et al.*[66] Eq. (23) shows that the dipole integral is a sum of products of vibrational and rotational factors and thus reveals the role of the vibrational dipole integral in the line strength. The vibrational dipole integral can be evaluated using

$$\begin{aligned}
\mu_{+1}^{\rm BF} &= \frac{-1}{\sqrt{2}}(\mu_x^{\rm BF} + i\mu_y^{\rm BF}) \\
\mu_0^{\rm BF} &= \mu_z^{\rm BF} \\
\mu_{-1}^{\rm BF} &= \frac{1}{\sqrt{2}}(\mu_x^{\rm BF} - i\mu_y^{\rm BF}) \qquad (24)
\end{aligned}$$

(following Ref. 58) and

$$\begin{aligned}
\mu_x^{\rm BF} &= \mu_1 \sin\theta_1 + \mu_2 \sin\theta_2 \cos\phi_2 \\
\mu_y^{\rm BF} &= \mu_2 \sin\theta_2 \sin\phi_2 \\
\mu_z^{\rm BF} &= \mu_1 \cos\theta_1 + \mu_2 \cos\theta_2 \qquad (25)
\end{aligned}$$

where $\mu_1 = \mu_2 = \mu_{\rm NNO}$. For example, the contribution to the vibrational dipole integral of $\mu_0^{\rm BF}$ from vector $\mathbf{r_1}$ is

$$\langle l_1'(m_1')l_2'm_2'|\mu_0^{\rm BF}|l_1(m_1)l_2m_2\rangle = \mu_1 \delta_{m_1',m_1}\delta_{l_2',l_2}\delta_{m_2',m_2}\langle Y_{l_1'}^{m_1}|\cos\theta_1|Y_{l_1}^{m_1}\rangle \qquad (26)$$

with

$$\langle Y_{l_1'}^{m_1}|\cos\theta_1|Y_{l_1}^{m_1}\rangle = \left[\frac{(l_1-m_1+1)(l_1+m_1+1)}{(2l_1+1)(2l_1+3)}\right]^{1/2}\delta_{l_1',l_1+1} + \left[\frac{(l_1-m_1)(l_1+m_1)}{(2l_1-1)(2l_1+1)}\right]^{1/2}\delta_{l_1',l_1-1} . \qquad (27)$$

The same contribution can be derived by simplifying Eq. (21). Finally, when computing the line strength, the summation over M and M' in Eq. (16) can be factored out and evaluated explicitly,

$$\sum_{M,M'} \begin{pmatrix} J' & 1 & J \\ -M' & 0 & M \end{pmatrix}^2 = \frac{1}{3} \qquad (28)$$

VI. RESULTS

A. Bright vibrational states

All vibrational states up to 190 cm^{-1} with $R(0)$ line strengths larger than 1.0 (all line strengths in this paper are reported in units of the NNO dipole) are given in Table II. All energy levels in this paper are with respect to the zero point energy (ZPE). We refer to these as bright states. Due to their brightness these states must have significant amplitude outside the non-polar well (see section IV B). This is confirmed by making probability density (PD) plots of each state. The PD plots are made by integrating out other coordinates. We made 2D plots for the coordinates pairs $(\theta_1, \theta_2), (\theta_2, \phi_2), (r_0, \theta_2), (r_0, \phi_2)$ and all 1D PD plots for each vibrational state. Fig. 6 shows very clean localized polar and TN states. The polar state has amplitude in the two polar wells at $(\theta_1 \sim 60°, \theta_2 \sim 60°)$ and $(\theta_1 \sim 120°, \theta_2 \sim 120°)$. The TN state has amplitude in the two TN wells at $(\theta_1 \sim 90°, \theta_2 \sim 0°)$ and $(\theta_1 \sim 180°, \theta_2 \sim 90°)$. Fig. 7 shows clean $v = 1$ and $v = 2$ torsion states in the polar well. The PD of the $v = 1$ torsion state in the nonpolar well has only one maximum but the PD of the polar $v = 1$ torsion state has two maxima because there are two polar wells (one near $\theta_2 = 60°$ and another near $\theta_2 = 120°$). In the nonpolar well the torsional vibration is about $\phi_2 = 180°$ and the $v = 1$ nonpolar torsion state therefore has a node at $\phi_2 = 180°$. On the other hand, the torsional vibration in the polar wells is about $\phi_2 = 0$ and the $v = 1$ polar torsion state has a node at $\phi_2 = 0$. Fig. 8 shows geared (disrotatory) states for both the nonpolar and polar cases. The geared coordinate in the polar well is $\delta\theta_1 - \delta\theta_2(A+)$ and the geared coordinate in the non-polar well is $\delta\theta_1 + \delta\theta_2(B+)$. The differences in symmetry and the direction of the motion of the two types of geared coordinates are clearly apparent in Fig. 8. However, the two geared modes in both wells are both along the disrotatory valley, as is clearly seen in Fig. 2 using extended angles. Fig. 9 shows a special state (cf. next section). It is the 20th $A-$ state and is assigned as a combination of torsion+gear in the polar wells. This state is special because its $\Delta K_a = 0$ transition is much weaker than that of all other bright vibrational states. All of these figures clearly demonstrate that there are wavefunctions that are well localized in the polar wells. This is consistent with the observation of the rotational spectrum of the polar isomer. There are also states, see Fig. 10, that have amplitudes in both the polar and the TN wells. The 31th and 35th $A+$ states in Fig. 10 have primarily

disrotatory and stretch character.

B. Analysis of vibration-rotation-tunnelling levels

An experimental rotational spectrum of the polar isomer was observed several years ago[4]. There are actually two polar wells and it is therefore in principle possible to study the tunnelling between them. We find that the tunnelling in the first five polar-like and TN-like states ground state is tiny (Table II). The smallness of the splitting is primarily due to the mass that is moved as the molecule tunnels. When tunnelling splitting is larger, e.g., in HF dimer, it is mostly hydrogen atoms that move.

Despite the smallness of the splitting, we would like to determine whether rovibrational transitions occur *across* tunnelling states or *within* a tunnelling state. For a transition within tunnelling states the initial state is associated with the lower (upper) tunnelling partner and the final state is also associated with the lower (upper) tunnelling partner. For a transition across tunnelling states the initial state is associated with the lower (upper) tunnelling partner and the final state is associated with the upper (lower) tunnelling partner. For HF dimer this was analysed by Mills[34] and by Hougen and Ohashi[33]. In the HF dimer case, because one path is dominant, it is even possible to determine which path is dominant, once it is known whether transitions occur within or across. For NNO dimer this is not possible because there are several competing paths.

If the tunnelling splitting is not tiny then one can distinguish between the within and across cases. In the within case the two $R(0)$ tunnelling transitions have very similar frequencies. In the across case the two $R(0)$ tunnelling transition frequencies are different. In NNO dimer the splitting is so small that the upper $\rightarrow$ lower and lower $\rightarrow$ upper transition frequencies are essentially the same. We know only that a bright $R(0)$ transition is between two levels associated with the same vibrational state. To establish if a bright transition is within or across we determine the vibrational parent (in this context a vibrational label includes both a vibrational state label and a tunnelling state label) of the $J = 1$ state to which the transition occurs. Vibrational parents for the bright $J = 1$ levels are shown in Table III. As can be seen from this table, all $J = 1$ levels can be assigned to a tunnelling state with a large value of P_v.

Even for a non-rigid molecule, to the extent that a vibrational/rotational factorization of the wavefunction is possible, one can determine symmetries of rotational functions for each vibrational state. Knowing the symmetry of a $J > 0$ state and the symmetry of its vibrational parent and using the product rule, $\Gamma_{vr} = \Gamma_v \Gamma_r$ (Γ_v includes Γ_{tunnel} here), we determine the symmetry of the rotational factor, Γ_r. Γ_r for $J = 1$ levels are given in Table IV. The results fall into two cases, as summarized in Table IV. These Γ_r can be compared with what one would obtain if the molecule were rigid. When a molecule is rigid the symmetry of the rotational wavefunctions can be determined from its point group. For a rigid molecule the evenness and oddness of $K_a K_c$ determine the symmetry of the rotational functions, as we have shown in Table IV for two rigid shapes having point group symmetry C_{2h} and C_{2v}[19, 33].

The $J = 1$ levels whose vibrational parents are one of the 11 nonpolar vibrational states (Table VII of paper I) are all case (a) (see Table IV). Case (a) is exactly what one would expect for a rigid molecule of C_{2h} symmetry. The nonpolar isomer has C_{2h} symmetry and the fact that we observe case (a) for nonpolar parents is therefore consistent with the idea that nonpolar wavefunctions have significant amplitude close to the nonpolar minimum. Because Γ_r of case (a) can only be $B-$ or $A+$ (true not only for $J = 0$ and 1, but for all J) and the dipole symmetry is $A-$, symmetry ensures that there are no pure rotational transitions. Γ_r is a consequence of the vibrational parent, therefore, rotational transitions can occur only if coupling is strong enough to change parents and hence convert rovibrational levels from case (a) to case (b).

We find that rovibrational transitions between the non-polar ground state and the non-polar torsional state have appreciable intensity. For example, the c-type $R(0)$ transition between the $\Gamma_{vr} = A+$, 0_{00} ground state at E = 0.0 cm^{-1} and the $\Gamma_{vr} = A-$, 1_{10} $v = 1$ torsion state at E = 26.1093 cm^{-1} is symmetry-allowed, see Table VII of paper I. This is consistent with the fact that Dehghany *et al.* [2] observed c-type transitions in the torsion + in-phase NNO monomer ν_1 stretch infrared combination band of the non-polar isomer. To the extent that the line strength of the combination band and the torsion fundamental are similar, the line strength we compute, $S = 0.033$ (see also Table IX), should be close to the measured line strength in Dehghany *et al.*'s experiment. Indeed, Dehghany *et al.* observe that this c-type band is 20 times weaker than the NNO dimer fundamental band.

Rotational functions of almost all the bright states belong to case (b); the only exceptions are states $A+(21)$ and $A-(20)$. These bright states include polar states and TN states. All bright R(0) transitions are given in Table V and some bright $Q(1)$ transitions are given in Table VI. The R(0) and Q(1) transitions for case (b) are illustrated in Fig. 11. Each vibrational state has two $R(0)$ transitions and each of these is a doublet due to the very small tunnelling splitting. Each vibrational state also has two $Q(1)$ transitions and each is a doublet. Many of the bright vibrational states have two upper rovibrational states, $(1_{11}, A-)$ and $(1_{01}, A-)$, linked with the $(0_{00}, A+)$ level by R(0) transitions. These two upper states are the lower states of two Q(1) transitions to a common upper state $(1_{10}, A+)$. For case (b), all the R(0) and Q(1) bright transitions in the lists can be linked in this way. From Fig. 11 one can clearly conclude that in case (b) the $\Delta K_a = 1$ transitions are *within* the same tunnelling state and the $\Delta K_a = 0$ transitions are *across* two tunnelling states. To extract this information from the results, one must use the vibrational parent analysis since on the basis of the strength of a transition one can deduce only that the lower and upper levels share the same vibrational state, and not which tunnelling component to associate with the two levels. Case (b) is exactly what one would expect if the molecule were rigid and had C_{2v} symmetry. Neither of the polar equilibrium geometries is C_{2v}, but there is a 1-D tunnelling path, between the two polar minima, that crosses the curve along which NNO dimer is C_{2v}, and is close to the minimized conrotatory path in figure 4. If tunnelling along one path were dominant one could use the symmetry of the rotational factors to determine the symmetry of that path. This is discussed by Hougen and Ohashi for HF dimer. [33] A similar analysis for NNO dimer is not possible (or necessary) because there are several competing tunnelling paths.

The two vibrational bright states that are not formally case (b) are $A+(21)$ and $A-(20)$. Their Γ_r differ from those of case (b) (Table IV) because the Γ_r of the $J = 1$ levels with the highest energies (both $K_a = 1$ levels) are interchanged. These two higher levels are close because the averaged geometry in NNO dimer polar states is nearly prolate (A is much larger than B and C). Owing to the fact that they are close small rovibrational perturbations could change their order. Thus although $A+(21)$ and $A-(20)$ are not strictly case (b), they are very nearly case (b) and $\Delta K_a = 1$ and $\Delta K_a = 0$ transitions are, as is true for case (b) states, *within* or *across*, respectively, tunnelling states. The $A-(20)$ vibrational state is different

from all other bright vibrational states in Table V and VI in that while each of the other vibrational states has two bright $R(0)$ transitions, the $A-(20)$ state has only one bright $R(0)$ transition and it is a $\Delta K_a = 1$ transition. It also has only one bright $\Delta K_a = 1$ $Q(1)$ transition. The missing $\Delta K_a = 0$ transition does exist, but its line strength is much weaker. For example, the line strength of the $\Delta K_a = 0$ R(0) transition of $A-(20)$ is $S = 0.11$. This may be compared with the strong $\Delta K_a = 1$ R(0) transition with $S = 3.14$ given in Table V. The quenching of the $\Delta K_a = 0$ transition indicates that the vibrationally averaged dipole component along the inter-monomer axis is small. It is somewhat surprising that this happens in a clean torsion+gear polar state and not in other lower states (the polar $v = 1$ torsion state for example). Simultaneous excitation of multiple vibrational modes may play a role here. If one adopts asymmetric top notation, one would consider the strong R(0) and Q(1) transitions of $A-(20)$ c-type transitions, while the corresponding lines for all other bright states are b-type transition. Interchanging the two highest $J = 1$ rotational levels changes a transition from b-type to c-type. Given the closeness of these two levels, one should not attach much significance to the distinction between b-type and c-type transitions.

We also assign high J levels of the ground state of the polar isomer in order to compare with the MW experiment[4]. A good procedure is to calculate only the Q-branch because all the $2J+1$ levels (each of which is doubly degenerate due to tunnelling) will be involved in the Q(J) bright transitions (Fig. (11b)). Because the tunnelling splitting is so small we use the vibrational parent analysis to determine which of two nearly degenerate rovibrational levels is associated with the A+ tunnelling state. Their Γ_{vr} are listed in Table VII. Again a dominant vibrational parent can always be found, however, P_v does tend to decrease with increasing J. Note that for levels in Table VII the Γ_r are determined by the evenness and oddness of $K_a K_c$.

In Table VIII, the MW lines of Walter *et al.* [4] are compared with the calculated lines. The differences are on the order of 0.001 cm^{-1}. Despite the precision of modern MW experiments it seems unlikely that it is possible to resolve the components of the tunnelling doublets. The splitting is $\sim 5 \times 10^{-8}$ cm^{-1} for the 0_{00} polar level and $\sim 9 \times 10^{-9}$ cm^{-1} for the 1_{11} polar level. Of course it is possible that in higher bright states the splitting is large enough that it would be observable. According to the potential we use there are states localized in the TN wells. Some lower level ab initio calculations do not predict TN wells. If

experimentalists could confirm the existence of the TN states this would confirm the superior accuracy of the higher level ab initio calculations. Rotational energy levels of the symmetric tunnelling partner of the TN ground state are in a table in supplementary material.

It is striking that all the bright transitions are within a vibrational state (the tunnellng states may be different). Transitions between *different* vibrational states are usually weak, even when they are symmetry-allowed. Line strengths for such transitions from the non-polar ground state or the polar ground state to other states are given in Table IX. The observed [2] transition from the non-polar ground state to the non-polar torsion state, discussed previously, is the strongest band in Table IX. The inter-vibration bands for the polar isomers are two to three orders of magnitude weaker. It is therefore unlikely that these bands will be observed.

VII. CONCLUSION

In this paper we have studied NNO dimer states localized in polar and T-shaped N-in wells and transitions between the states. Despite the fact that hundreds of thousands of basis functions are required to determine converged energy levels it is not computationlly difficult to compute a list of energy levels. It is easily done with the Lanczos algorithm and evaluating potential matrix-vector products by using quadrature and doing sums sequentially. A list of energy levels, however, does not provide much understanding. One can attach symmetry and J labels to the levels but it is hard to identify rovibrational states that can be associated with the nonpolar, polar and TN wells.

In this paper we use two tools for identifying what we call the vibrational parent of a rovibrational state. This enables us to systematically link rovibrational and vibrational states and hence to find the states in energy level lists that correspond to polar-like and TN-like vibrational states. In the first procedure we expand rovibrational states in terms of vibrational wavefunctions (section IVA). In the second procedure (section IVB) we use intensity to identify bright transitions and hence find the polar-like rovibrational states. Both of these procedures are systematic and easy to use. They do not require making and interpreting plots. It would be labourious to make and inspect plots of thousands of wavefunctions. By determining vibrational parents we are able to break the rovibrational

states into two groups: class (a) and class (b). There are no rotational transitions between states of class (a) with the same vibrational parent. These are dark states. Their vibrational parents all have amplitude concentrated in the non-polar well. There are strong rotational transitions between class (b) states with the same vibrational parent (but the tunnelling state may be different). These are bright states. Their vibrational parents all have amplitude concentrated in the polar wells or the TN wells. We find that transitions between states having different parents are all weaker than transitions between states with the same (bright) parents. The vibrational parent analysis also enables us to determine whether rovibrational transitions occur between the same or different tunnelling partners. When the tunnelling splitting is not tiny (e.g HF dimer) the vibrational parent analysis is not necessary, but in NNO dimer it is necessary because the splittings are $\sim 10^{-8}$ cm^{-1}.

Zheng *et al.* [14] have done calculations similar to ours but on a different potential surface. Their potential points are computed at the CCSD(T)/aug-cc-pVTZ level. They report energies for the polar ground state ($J \geq 0$) and all four fundamental bands of the polar isomer(s). Although the polar ground state energy of Zheng *et al.* (137.0 cm^{-1}) differs somewhat from our value (143.5 cm^{-1}), the vibrational energies of the geared and torsion states measured from the polar ground state are very close : 20.3 cm^{-1} and 21.4 cm^{-1} for our calculation, and 20.1 cm^{-1} and 21.3 cm^{-1} for Ref. 14. Zheng *et al.* assigned a stretch polar state at 44.2 cm^{-1}. Two of our calculated bright vibrational states near this energy, (states $A + (31)$ and $A + (35)$ in Table II and Fig. 10), have stretch excitation, but their (θ_1, θ_2) PD plots show that neither is a pure stretch state. The four fundamentals of the non-polar states of Ref. 14 agree with our results reported in paper I to within 2.4 cm^{-1}. Zheng *et al.* did not find TN states presumably because their potential surface has no or very shallow TN minima. They do not explain how they identify $J > 0$ polar states but do report $J > 0$ levels of the polar ground state. The two tools we propose make it possible to do this in a systematic fashion and it should be possible to use them to disentangle and analyze lists of energy levels for many molecules.

Acknowledgments

This work has been supported by the Natural Sciences and Engineering Research Council of Canada. Calculations were done on computers of SciNet.

---

[1] M. Dehghany, M. Afshari, Z. Abusara, N. Moazzen-Ahmadi and A. R. W. McKellar, J. Chem. Phys. **126**, 164310 (2007)

[2] M. Dehghany, M. Afshari, N. Moazzen-Ahmadi and A. R. W. McKellar, Phys. Chem. Chem. Phys. **10**, 1658 (2008)

[3] M. Dehghany, M. Afshari, R. I. Thompson, N. Moazzen-Ahmadi, and A. R. W. McKellar, J. Mol. Spectrosc. 252, 1 (2008).

[4] N. R. Walker, A. J. Minei, S. E. Novick, and A. C. Legon, J. Mol. Spectrosc. **251**, 153 (2008)

[5] M. Dehghany, M. Afshari, Z. Abusara and N. Moazzen-Ahmadi, Phys. Chem. Chem. Phys. **11**, 7585 (2009)

[6] Y. Ohshima, Y. Matsumoto, M. Takami, and K. Kuchitsu, Chem. Phys. Lett. 152, 294 (1988).

[7] H. B. Qian, W. A. Herrebout, and B. J. Howard, Mol. Phys. 91, 689 (1997).

[8] M. Dehghany, M. Afshari, Z. Abusara, C. Van Eck and N. Moazzen-Ahmadi, J. Mol. Spectrosc. **247**, 123 (2008)

[9] G. M. Berner, A. L. L. East, M. Afshari, M. Dehghany, N. Moazzen-Ahmadi, and A. R. W. McKellar, J. Chem. Phys. **130**, 164305 (2009)

[10] Mogi, T. Komine, and K. Hirao, J. Chem. Phys. 95, 8999 (1991).

[11] C. Dutton, A. Sazonov, and R. A. Beaudet, J. Phys. Chem. 100, 17772 (1996)

[12] H. Vald?s and J. A. Sordo, J. Phys. Chem. A 108, 2062 (2004).

[13] R. Dawes, X.-G. Wang, A. W. Jasper and T. Carrington, Jr. J. Chem. Phys. **133**, 134304 (2010)

[14] Limin Zheng, Yunpeng Lu, Soo-Ying Lee, Hong Fu, and Minghui Yang, J. Chem. Phys. 134, 054311 (2011)

[15] A.R. W. McKellar, H. L. Welsh, J. Chen. Phys. 55, 595 (1971).

[16] J. Tang, Y. Xu, A. R. W. McKellar, and W. Jager, Science 297, 2030 (2002)

[17] Y. Xu, W. Jager, J. Tang, and A. R. W. McKellar, Phys. Rev. Lett. 91, 163401 (2004)

[18] J. Tang and A. R. W. McKellar, J. Chem. Phys. 117, 2586 (2002).

[19] P. R. Bunker and P. Jensen, *Molecular Symmetry and Spectroscopy* (NRC Research Press: Ottawa 1998).

[20] P. Jensen and P. R Bunker, editors: Computational Molecular Spectroscopy, Wiley, Chichester, 2000

[21] A. L. East and P. R. Bunker, Chem. Phys. Lett. 282, 49-53 (1998)

[22] A. L. East, M. Kolbuszewski and P. R. Bunker, J. Phys. Chem. 101, 6746-6752 (1997)

[23] P. R. Bunker, P. Jensen, Y. Yamaguchi and H. F. Schaefer III, J. Mol. Spectrosc. 179, 263-268 (1996)

[24] P.R. Bunker, T. Carrington Jr., P.C. Gomez, M.D.Marshall, M. Kofranek, H. Lischka, and A. Karpfen, J. Chem. Phys. 91, 5154-5159 (1989)

[25] Per Jensen and P.R Bunker, J. Mol. Spectros. 99, 348-356 (1983)

[26] J.T. Hougen, P.R. Bunker, and J.W.C. Johns, J. Mol. Spectrosc. 34, 136-172 (1970)

[27] P.R Bunker, Ann. Rev. Phys. Chem. 34,59-75 (1983)

[28] T. B. Adler, G. Knizia, and H.-J. Werner, J. Chem. Phys. 127, 221106 (2007)

[29] X. Chapuisat and C. Iung, Phys. Rev. A **45**, 6217 (1992)

[30] X.-G. Wang and T. Carrington Jr., J. Chem. Phys. **118**, 6946 (2003)

[31] X.-G. Wang and T. Carrington Jr., J. Chem. Phys. **121**, 2937 (2004).

[32] F. Gatti, C. Iung, M. Menou, Y. Justum, A Nauts, and X Chapuisat, J. Chem. Phys., **108**, 8804. (1998)

[33] J. T. Hougen and N. Ohashi, J. Mol. Spectrosc. **109**, 134 (1985)

[34] I. M. Mills, J. Phys. Chem. **88**, 532 (1984)

[35] X.-G. Wang, T. Carrington Jr., J. Tang, and A. R. W. McKellar, J. Chem. Phys. **123**, 034301 (2005)

[36] J. C. Light, I. P. Hamilton, and J. V. Lill J. Chem. Phys. **82**, 1400 (1985)

[37] J. C. Light and T. Carrington Jr., Adv. Chem. Phys. **114**, 263 (2000)

[38] Z. Bacic and J. C. Light, Annu. Rev. Phys. Chem. **40**, 469 (1989)

[39] R. G. Littlejohn, M. Cargo, T. Carrington Jr. , K. A. Mitchell, and B. Poirier J. Chem. Phys. **116**, 8691 (2002)

[40] H. Wei and T. Carrington Jr., J. Chem. Phys. **97**, 3029 (1992).

[41] J. Echave and D. C. Clary, Chem. Phys. Lett. **190**, 225 (1992).

[42] X.-G. Wang and T. Carrington Jr, J. Chem. Phys. **114**, 1473 (2001).

[43] R. Chen and H. Guo, J. Chem. Phys. **114**, 1467 (2001).

[44] X.-G. Wang and T. Carrington Jr., J. Chem. Phys. **115**, 9781 (2001)

[45] J. K. Cullum and R. A. Willoughby, *Lanczos algorithms for large symmetric eigenvalue computations*, (Birkhäuser, Boston, 1985).

[46] M. J. Bramley and T. Carrington Jr., J. Chem. Phys. **99** , 8519 (1993).

[47] M. J. Bramley and T. Carrington Jr., J. Chem. Phys. **101**, 8494 (1994).

[48] R. Chen, G. Ma, and H. Guo, J. Chem. Phys. **114**, 4763 (2001)

[49] X.-G. Wang and T. Carrington Jr., J. Chem. Phys. **119**, 101 (2003)

[50] M. J. Bramley, J. W. Tromp, T. Carrington, Jr., and G. C. Corey, J. Chem. Phys. **100**, 6175 (1994)

[51] T. Carrington Jr., *Encyclopedia of Computational Chemistry*, editor-in-chief Paul von Ragué Schleyer, volume **5**, (John Wiley & Sons, 1998).

[52] R. Chen and H. Guo, J. Chem. Phys. **108**, 6068 (1998).

[53] X.-G. Wang and T. Carrington Jr, J. Chem. Phys. **117**, 6923 (2002).

[54] X.-G. Wang, and T. Carrington, Jr. J. Phys. Chem. A **111**, 10220 (2007)

[55] G. A. Blake, K. L. Busarow, R. C. Cohen, K. B. Laughlin, Y. T. Lee, and R. J. Saykally, J. Chem. Phys. **89**, 6577 (1988)

[56] E. Matyus, C. Fabri, T. Szidarovszky, G. Czako, W. D. Allen, and A. G. Csaszar, J. Chem. Phys. **133**, 034223 (2010).

[57] X.-G. Wang and T. Carrington Jr, J. Chem. Phys. **134**, 044313 (2011).

[58] R. N. Zare, *Angular Momentum* (Wiley: New York 1988).

[59] G. Brocks, A. van der Avoird, B. T. Sutcliffe, and J. Tennyson, Mol. Phys. **50**, 1025 (1983).

[60] S. C. Althorpe and D. C. Clary, J. Chem. Phys. **101**, 3603 (1994).

[61] S. C. Smith, Chem. Phys. Lett. **243**, 359 (1995).

[62] H. Chen, S. Liu, and J. C. Light, J. Chem. Phys. **110**, 168 (1999).

[63] M.. J. Elrod and R. J. Saykally, J. Chem. Phys. **103**, 921 (1995).

[64] A. van der Avoird, P. E. S. Wormer, and R. Moszynski, Chem. Rev. **94**, 1931 (1994).

[65] G. W. M. Vissers, G. C. Groenenboom, and A. van der Avoird, J. Chem. Phys. **119**, 286 (2005).

[66] C. R. Le Sueur, S. Miller, J. Tennyson and B. T. Sutcliffe, Mol. Phys. **76**, 1147 (1992).

TABLE I: Stationary point energies (in cm^{-1}) on the IMLS fitted potential. NO stands for non-polar-O-in. It is also labelled as G because it is global minimum. See texts for notations for other points. ΔE is the difference from the energy of the polar well.

	NO	TO	P	TN	NN	RT
E	-633.43	-360.21	-465.20	-421.03	-322.85	-65.71
ΔE	-168.23	104.99	0.00	44.17	142.35	399.49

TABLE II: Bright vibrational levels (in cm^{-1}) of $(NNO)_2$ less than 190 cm^{-1} above the zero point energy (ZPE). The energy is measured relative to the ZPE which is -514.21180 cm^{-1}. g.s. stands for the ground state. The levels occur in pairs. Wavefunctions for levels denoted E_s (E_a) are symmetric (antisymmetric) with respect to exchange of the monomers. The number in parenthese in the second and third columns is the ordinal number within the symmetry block.

assignment	sym of E_s	sym of E_a	E_s	E_a	$\Delta = E_a - E_s$
polar g.s.	$A+(12)$	$B+(9)$	143.52941	143.52941	0.00000
polar + gear	$A+(21)$	$B+(13)$	163.84179	163.84179	0.00000
polar + torsion	$A-(13)$	$B-(9)$	164.92546	164.92546	0.00000
[a]	$A+(25)$	$B+(15)$	173.29199	173.29200	0.00001
TN g.s.	$A+(26)$	$B+(19)$	178.02947	178.02947	0.00000
polar + torsion + gear	$A-(20)$	$B-(12)$	183.84371	183.84508	0.00137
polar + torsion overtone	$A+(30)$	$B+(23)$	184.76743	184.76595	-0.00148
mixture (polar + TN)	$A+(31)$	$B+(24)$	185.18691	185.18676	-0.00015
mixture (polar + TN)	$A+(35)$	$B+(25)$	188.18546	188.17448	-0.01098

[a] This is a polar state with structure in the geared, anti-geared, and stretch coordinates.

TABLE III: $J = 1$ levels of the bright vibrational states of Table II. The assignments are based on both the vibrational parent analysis and the intensity calculation. The tunnelling splitting for the first five vibrational states is smaller than 0.0001 cm^{-1} and therefore the energy of the asymmetric tunnelling state is not listed. Each $J = 1$ level is labelled by (sym,P_v), where P_v is computed from Eq. (5). The $J = 0$ levels are labelled by (sym, ordinal number).

0_{00}	1_{01}	1_{11}	1_{10}
143.52941 $(A+,12)$	143.62998($B-$,0.98)	143.88389($A-$,0.97)	143.89221($B+$,0.99)
163.84180 $(A+,21)$	163.93025($B-$,0.99)	164.10161($B+$,0.89)	164.10437($A-$,0.90)
164.92546 $(A-,13)$	165.03010($B+$,0.95)	165.39156($A+$,0.83)	165.40051($B-$,0.87)
173.29199 $(A+,25)$	173.38387($B-$,0.99)	173.66508($A-$,0.96)	173.67155($B+$,0.97)
178.02947 $(A+,26)$	178.10566($B-$,1.00)	178.46832($A-$,0.82)	178.47215($B+$,0.82)
183.84371 $(A-,20)$	183.90535($B+$,0.81)	183.97459($B-$,0.75)	184.00771($A+$,0.66)
183.84508 $(B-,12)$	183.90599($A+$,0.81)	183.97468($A-$,0.78)	184.00817($B+$,0.68)
184.76743 $(A+,30)$	184.87454($B-$,0.93)	185.32105($A-$,0.66)	185.32809($B+$,0.72)
184.76595 $(B+,23)$	184.87305($A-$,0.93)	185.32036($B-$,0.70)	185.32741($A+$,0.75)
185.18691 $(A+,31)$	185.27226($B-$,0.97)	185.57290($A-$,0.86)	185.57821($B+$,0.86)
185.18676 $(B+,24)$	185.27218($A-$,0.97)	185.56955($B-$,0.86)	185.57463($A+$,0.87)

TABLE IV: The symmetry of the $J = 1$ rotational factors, Γ_r, of $(NNO)_2$ obtained after removing Γ_v from Γ_{vr}. Γ_v is obtained from the symmetry of the vibrational parent of the rovibrational $J = 1$ wavefunctions. Two cases, denoted by a and b, are observed.

case of states	1_{01}	1_{11}	1_{10}
(a) Most dark states	$B-$	$B-$	$A+$
(b) Most bright states	$B-$	$A-$	$B+$
C_{2h} shape	$B-$	$B-$	$A+$
C_{2v} shape	$B-$	$A-$	$B+$

TABLE V: All bright $R(0)$ transitions (line strength $S > 1.0$) in cm^{-1} with lower state energies up to 190 cm^{-1}. Transitions originating from the symmetric (antisymmetric) tunnelling partner are on the left (right). Each vibrational/tunnelling state has two transitions $\Delta K_a = 0$ and $\Delta K_a = 1$ except for the state labelled by † whose $\Delta K_a = 0$ transition is weak. See Fig. (11a) for an illustration of transitions in this table.

sym ($J=0$)	$E_{J=0}$	$E_{J=1}$	Δ	S	sym ($J=0$)	$E_{J=0}$	$E_{J=1}$	Δ	S
$A+$	143.5294	143.6300	0.1006	1.4489	$B+$	143.5294	143.6300	0.1006	1.4489
$A+$	143.5294	143.8839	0.3545	2.4452	$B+$	143.5294	143.8839	0.3545	2.4452
$A+$	163.8418	163.9303	0.0885	1.0262	$B+$	163.8418	163.9303	0.0885	1.0262
$A+$	163.8418	164.1044	0.2626	2.5704	$B+$	163.8418	164.1044	0.2626	2.5704
$A-$	164.9255	165.0301	0.1046	1.6960	$B-$	164.9255	165.0301	0.1046	1.6960
$A-$	164.9255	165.3916	0.4661	1.9788	$B-$	164.9255	165.3916	0.4661	1.9788
$A+$	173.2920	173.3839	0.0919	1.4774	$B+$	173.2920	173.3839	0.0919	1.4776
$A+$	173.2920	173.6651	0.3731	2.2335	$B+$	173.2920	173.6651	0.3731	2.2335
$A+$	178.0295	178.1057	0.0762	1.3161	$B+$	178.0295	178.1057	0.0762	1.3161
$A+$	178.0295	178.4683	0.4389	1.4973	$B+$	178.0295	178.4683	0.4389	1.4973
$A-$	†183.8437	184.0077	0.1640	3.1429	$B-$	†183.8451	184.0082	0.1631	3.2476
$A+$	184.7674	184.8731	0.1056	1.6970	$B+$	184.7660	184.8745	0.1086	1.7021
$A+$	184.7674	185.3210	0.5536	1.5376	$B+$	184.7660	185.3204	0.5544	1.6202
$A+$	185.1869	185.2722	0.0853	1.2440	$B+$	185.1868	185.2723	0.0855	1.2616
$A+$	185.1869	185.5729	0.3860	1.9034	$B+$	185.1868	185.5696	0.3828	1.8970
$A+$	188.1855	188.2680	0.0826	1.2244	$B+$	188.1745	188.2784	0.1039	1.2244
$A+$	188.1855	188.5844	0.3990	1.4143	$B+$	188.1745	188.5962	0.4217	1.8094

TABLE VI: Bright $Q(1)$ transitions (in cm^{-1}) for two selected polar-like vibrational states, A+(12) and the polar + torsion + gear state, A-(20). $Q(1)$ transitions in this table are linked with the $R(0)$ transitions in Table V. See Fig. (11b) for an illustration of transitions in this table.

sym (E')	$E''_{J=1}$	$E'_{J=1}$	Δ	S	sym (E')	$E''_{J=1}$	$E'_{J=1}$	Δ	S
$A+$	143.6300	143.8922	0.2622	3.6677	$B+$	143.6300	143.8922	0.2622	3.6677
$A+$	143.8839	143.8922	0.0083	2.1732	$B+$	143.8839	143.8922	0.0083	2.1732
$A-$	183.9060	183.9747	0.0687	4.9280	$B-$	183.9054	183.9746	0.0692	4.8805

TABLE VII: Rotational energy levels of the symmetric tunnelling partner of the polar ground state (in cm^{-1}) up to $J = 3$. Energies of the rotational levels of the anti-symmetric partners are identical to within the figues presented and their symmetries are products of the symmetry in this table and $B+$. To determine which level is associated with the symmetric tunnelling partner we use the vibrational parent analysis.

J_{KaKc} Γ_{vr}	E	P_v
0_{00} $A+$	143.5294	1.00
1_{01} $B-$	143.6300	0.98
1_{11} $A-$	143.8839	0.97
1_{10} $B+$	143.8922	0.99
2_{02} $A+$	143.8309	0.94
2_{12} $B+$	144.0767	0.92
2_{11} $A-$	144.1017	0.97
2_{21} $B-$	144.8632	0.93
2_{20} $A+$	144.8634	0.93
3_{03} $B-$	144.1318	0.89
3_{13} $A-$	144.3658	0.84
3_{12} $B+$	144.4157	0.94
3_{22} $A+$	145.1650	0.88
3_{21} $B-$	145.1660	0.88
3_{31} $A-$	146.4547	0.86
3_{30} $B+$	146.4547	0.86

TABLE VIII: Rotation-tunnelling transitions (up to $J' \leq 2$) of the polar ground state (in cm^{-1}) of $(NNO)_2$. S is the calculated line strength.

$J''_{K''_a K''_c} \rightarrow J'_{K'_a K'_c}$	ν(cal)	ν(obs)	S
$0_{00} \rightarrow 1_{01}$	0.1006		1.45
$0_{00} \rightarrow 1_{11}$	0.3545	0.35510	2.45
$1_{10} \rightarrow 1_{01}$	0.2622	0.26325	3.67
$1_{10} \rightarrow 1_{11}$	0.0083		2.17
$1_{10} \rightarrow 2_{11}$	0.2095	0.20829	2.17
$1_{10} \rightarrow 2_{21}$	0.9710		3.67
$1_{01} \rightarrow 2_{02}$	0.2009	0.19988	2.90
$1_{01} \rightarrow 2_{12}$	0.4467	0.44694	3.67
$1_{11} \rightarrow 2_{02}$	0.0530		1.28
$1_{11} \rightarrow 2_{12}$	0.1928	0.19189	2.17
$1_{11} \rightarrow 2_{20}$	0.9796		3.61
$2_{11} \rightarrow 2_{02}$	0.2708	0.27166	6.01
$2_{11} \rightarrow 2_{12}$	0.0250		1.21
$2_{11} \rightarrow 2_{20}$	0.7618		2.14
$2_{21} \rightarrow 2_{12}$	0.7865		2.04
$2_{21} \rightarrow 2_{20}$	0.0002		4.83

TABLE IX: R(0) line strengths for transitions from the non-polar ground state or the polar ground state to other vibrational states.

v''	v'	assignment	ΔE (cm^{-1})	S
non-polar GS ($A+$)	non-polar torsion ($A-$)	$0_{00} \rightarrow 1_{01}$	26.1093	3.3E-2
non-polar GS ($A+$)	non-polar gear ($B+$)	$0_{00} \rightarrow 1_{01}$	41.9682	1.2E-2
non-polar GS ($A+$)	non-polar gear ($B+$)	$0_{00} \rightarrow 1_{11}$	42.2244	6.4E-3
polar GS ($A+$)	polar gear ($A+$)	$0_{00} \rightarrow 1_{01}$	20.4008	8.1E-5
polar GS ($A+$)	polar gear ($A+$)	$0_{00} \rightarrow 1_{10}$	20.5750	2.3E-4
polar GS ($A+$)	polar torsion ($A+$)	$0_{00} \rightarrow 1_{10}$	21.8711	2.1E-5

FIG. 1: Potential obtained by minimizing with respect to r_0 for (a) $\phi_2 = 180°$ and (b) $\phi_2 = 0°$. The contour interval is 60 cm^{-1} except the green contours (between -450 and -390 cm^{-1}) for which it is is 10 cm^{-1} and blue contours (between -70 and -60 cm^{-1}) for which it is 5 cm^{-1}. The green contours reveal the TN well and the blue contours reveal the rectangle-shaped (RT) transition state between the two polar monomer.

FIG. 2: Potential as a function of the extended angles $(\tilde{\theta}_1, \tilde{\theta}_2)$ obtained by minimizing with respect to r_0. The contour intervals are the same as in Fig. 1. The extended angle $\tilde{\theta}_1$ is defined as in Fig. 1 of paper I. The extended angle $\tilde{\theta}_2$ differs from the one defined in Fig. 1 of paper I: $\tilde{\theta}_2(\text{this work}) = \tilde{\theta}_2(\text{paper I}) - 180°$. The relation between $(\tilde{\theta}_1, \tilde{\theta}_2)$ and (θ_1, θ_2) is $\tilde{\theta}_1 = \theta_1$, $\tilde{\theta}_2 = \theta_2$ if $\phi_2 = 180°$, and $\tilde{\theta}_1 = \theta_1$, $\tilde{\theta}_2 = 360° - \theta_2$ if $\phi_2 = 0°$.

FIG. 3: The disrotatory cycle (solid arrow) starting from and ending at the global minimum (G). Two polar (P1) to polar (P2) tunnelling paths are indicated by the dashed arrows. The first one (disrotatory I) goes through TO1 and TO2 barriers (105 cm^{-1} higher than the polar wells) and the second one (disrotatory II) goes through a NN1 barrier (142 cm^{-1} higher than the polar wells).

FIG. 4: The conrotatory tunnelling path, going through an approximately rectangle-shaped (RT) barrier (400 cm^{-1} higher than the polar wells).

FIG. 5: Diagram illustrating how $J = 0$ and $J = 1$ bright states (in red) are identified by searching for bright $R(0)$ transitions. The two bright $R(0)$ transistions shown are from the polar ground state 0_{00} to the polar $J = 1$ excited states 1_{01} ($\Delta K_a = 0$) and 1_{11} ($\Delta K_a = 1$).

FIG. 6: Probability density plots for the ground state (E = 0 cm^{-1}, A+) (a), the polar ground state (E = 143.53 cm^{-1}, A+) (b) and the TN ground state (E =178.03cm^{-1}, A+) (c). The contour interval is 1.0.

FIG. 7: Probability density plots for the $v = 1$ torsion state in the polar wells (E = 164.93 cm^{-1}, A-) (b), the $v = 2$ torsion state in the polar wells (E = 184.77 cm^{-1}, A+) (c), and, as a comparison, the $v = 1$ torsion state in the non-polar well (E = 25.76 cm^{-1}, A-) (a). The contour interval is 0.4.

FIG. 8: Probability density plots for the $v = 1$ geared state in the polar wells (E = 163.84 cm^{-1}, B+) (b), and, as a comparison, the $v = 1$ geared state in the non-polar well (E = 41.86 cm^{-1}, B+) (a). The contour interval is 0.4.

FIG. 9: Probability density plots for the $A-(20)$ state (E = 183.84 cm^{-1}, $A-$). The contour interval is 0.4, 0.02 and 0.002 for (a), (b) and (c), respectively.

FIG. 10: Probability density plots for two mixture states that have amplitude in both the polar and the TN well. (a) is (E = 185.19 cm^{-1}, $A+$,31) and (b) is (E = 188.19 cm^{-1}, $A+$,35), The contour interval is 0.2.

FIG. 11: Transitions for Case (b) which includes most bright vibrational states including polar and TN states. The levels associated with the symmetric and anti-symmetric tunnelling states are on the left (solid lines) and right (dashed lines), respectively.

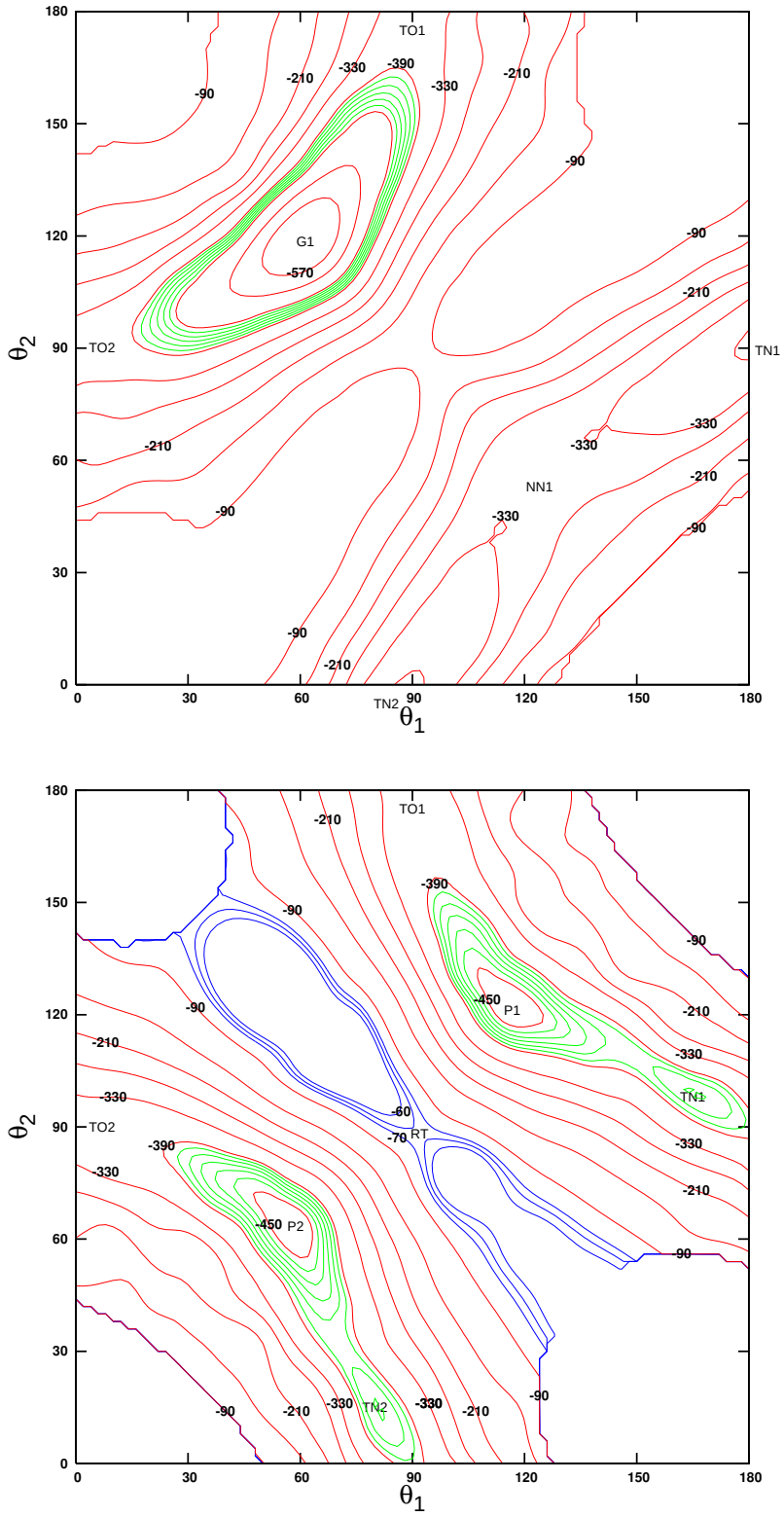

FIG. 1:

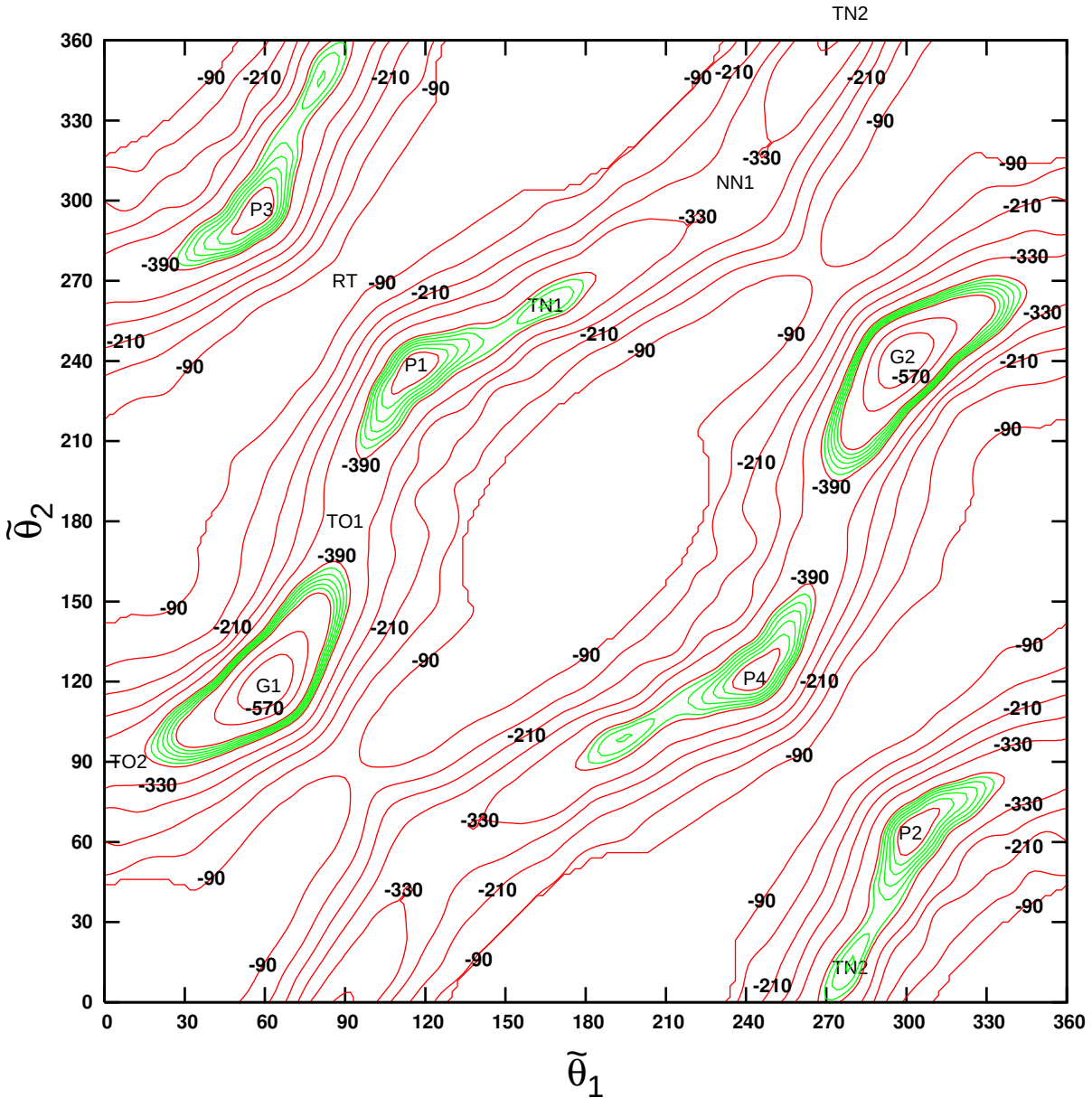
TN2
NN1
P3
RT
TN1
P1
G2
-570
TO1
G1
-570
TO2
P4
P2
TN2
$\tilde{\theta}_2$
$\tilde{\theta}_1$
0
30
60
90
120
150
180
210
240
270
300
330
360

FIG. 2:

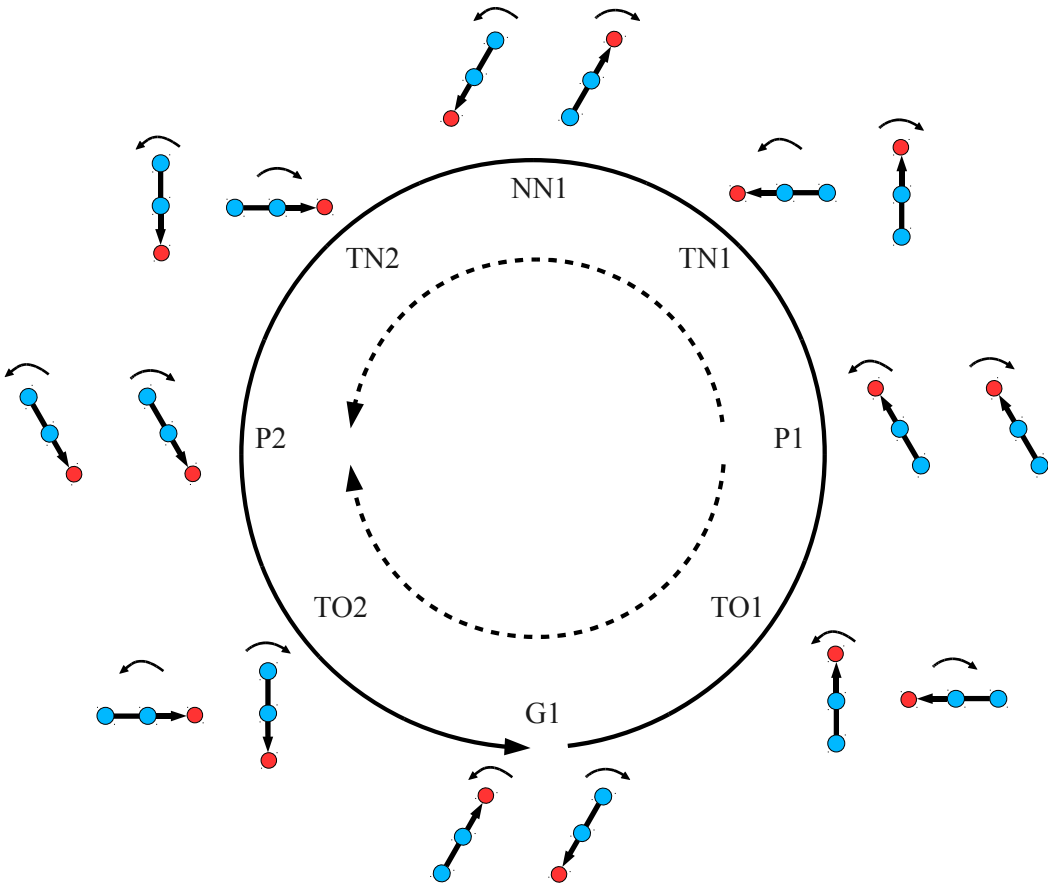

FIG. 3:

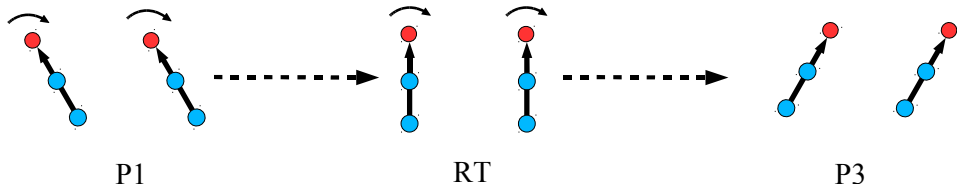

FIG. 4:

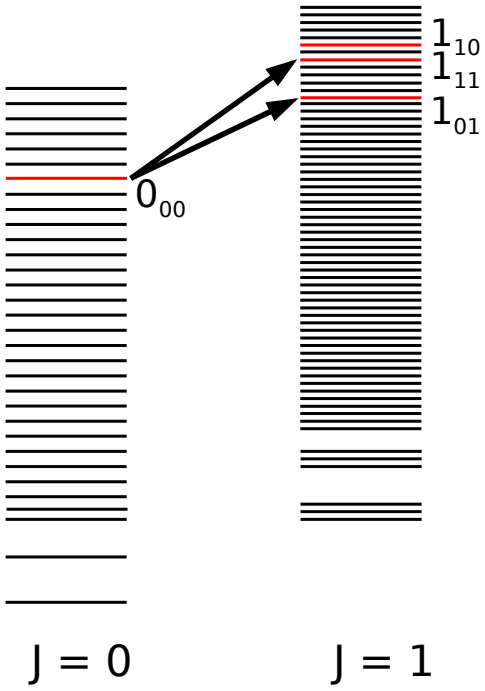

FIG. 5:

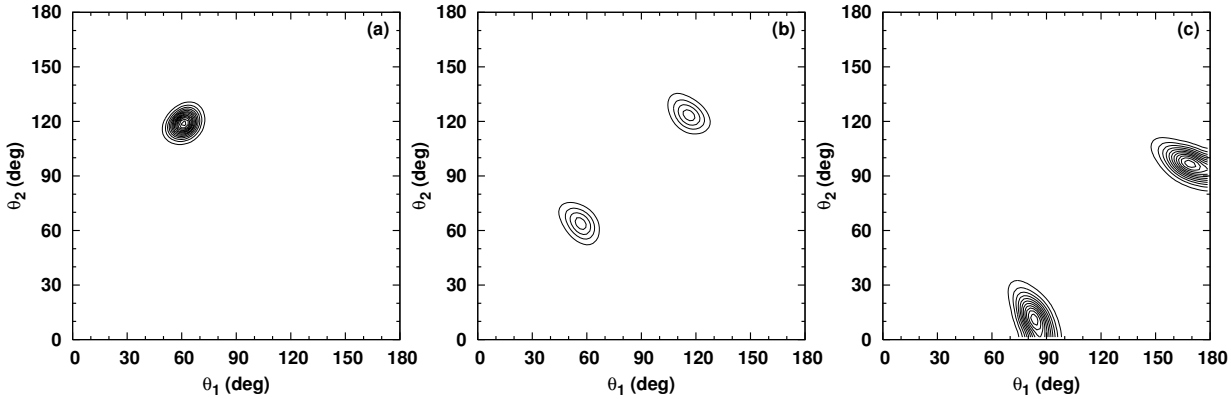
(a)
(b)
(c)
θ2 (deg)
θ1 (deg)
0
30
60
90
120
150
180

FIG. 6:

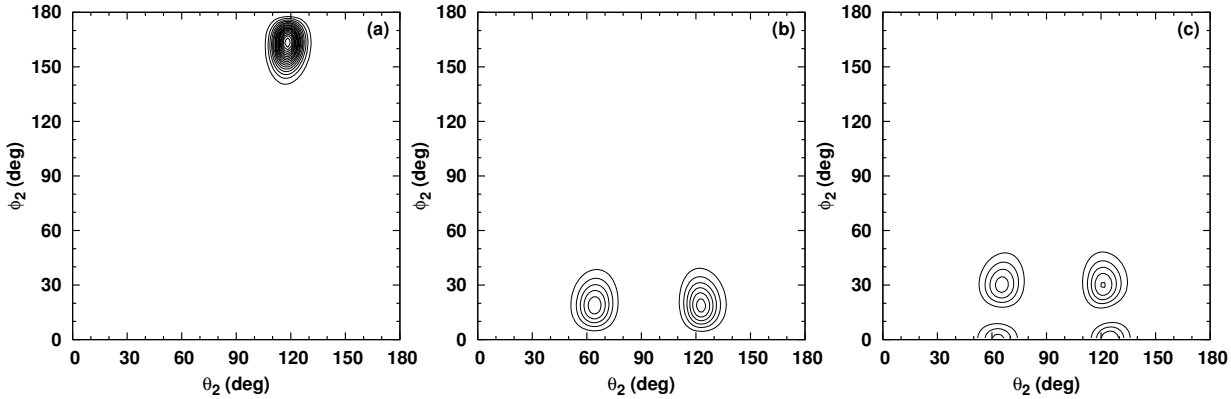
(a)
(b)
(c)
ϕ2 (deg)
θ2 (deg)
0
30
60
90
120
150
180

FIG. 7:

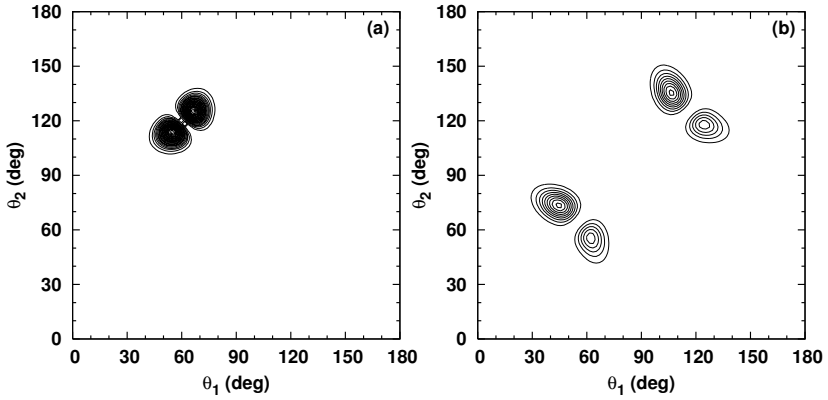

FIG. 8:

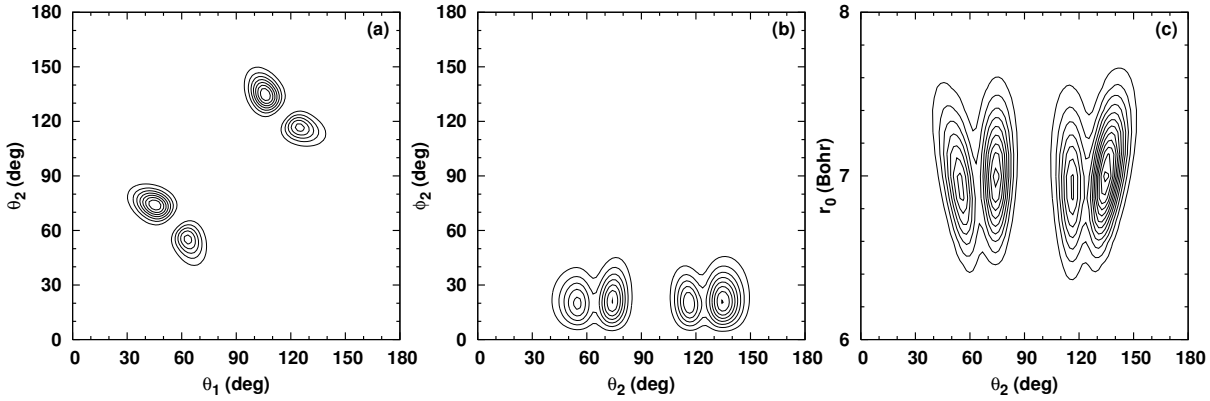

FIG. 9:

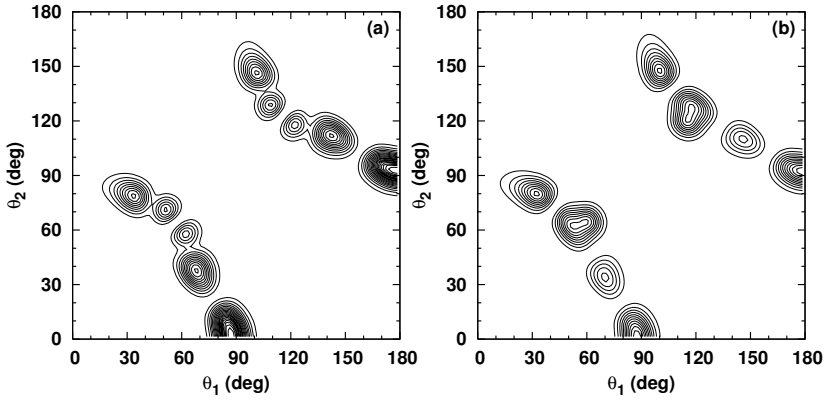

FIG. 10:

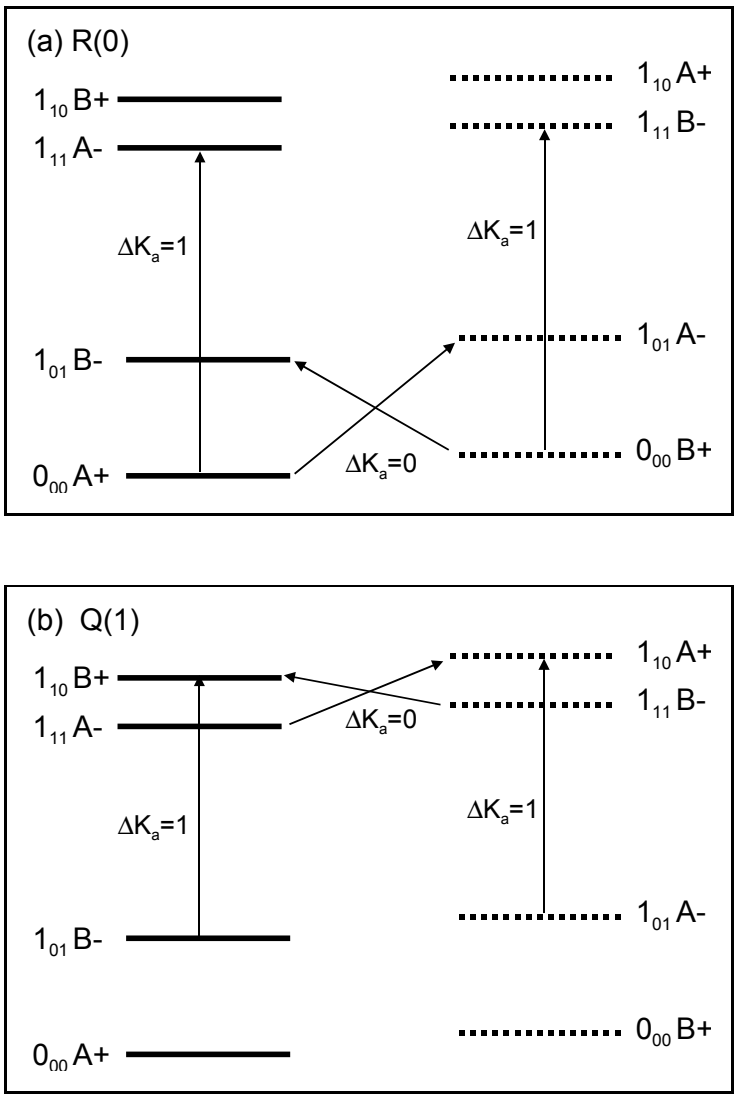
(a) R(0)
1_{10} B+
1_{11} A-
1_{01} B-
0_{00} A+
ΔK_a=1
ΔK_a=0
1_{10} A+
1_{11} B-
ΔK_a=1
1_{01} A-
0_{00} B+
(b) Q(1)
1_{10} B+
1_{11} A-
1_{01} B-
0_{00} A+
ΔK_a=1
ΔK_a=0
1_{10} A+
1_{11} B-
ΔK_a=1
1_{01} A-
0_{00} B+

FIG. 11: